Selective enhancement of infrared absorption with metal hole arrays

Yoshiaki Nishijima,[1,*] **Hiroki Nigorinuma,**[1] **Lorenzo Rosa,**[2] **and Saulius Juodkazis**[2,3]

[1]*Department of Electrical and Computer Engineering, Graduate School of Engineering, Yokohama National University, 79-5 Tokiwadai, Hodogaya-ku, Yokohama 240-8501, Japan*
[2]*Centre for Micro-Photonics, Faculty of Engineering and Industrial Sciences, Swinburne University of Technology, Hawthorn, VIC 3122, Australia*
[3]*Melbourne Centre for Nanofabrication, 151 Wellington Road, Clayton, VIC 3168, Australia*

[*]*nishijima@ynu.ac.jp*

Abstract: We use a surface-enhanced infrared absorption (SEIRA) spectroscopy, a useful sensing and surface analysis method complimentary to the Raman scattering spectroscopy, for the individual enhancement of specific molecular vibration bands and fingerprinting of molecular vibrations. SEIRA spectroscopic measurement using the metal hole array (MHA) is demonstrated with high spectral selectivity. The molecular IR absorption peaks are enhanced up to 10 times at the transmission peak of MHA structure when electromagnetic field enhancement is localized on the walls inside the holes. Experimental and numerical simulations results are in a good qualitative agreement. Selective IR band enhancement can be used for identification of specific molecules within complex mixtures and it can be extended to the longer wavelengths at THz molecular bands.

OCIS codes: (240.6680) Surface plasmons; (240.6490) Spectroscopy, surface; (300.6270) Spectroscopy, far infrared.

References and links

1. H. Nakanishi, K. J. M. Bishop, B. Kowalczyk, A. Nitzan, E. A. Weiss, K. V. Tretiakov, M. M. Apodaca, R. Klajn, J. F. Stoddart, and B. A. Grzybowski, "Photoconductance and inverse photoconductance in films of functionalized metal nanoparticles," Nature **460**, 371–375 (2008).
2. T. Rindzevicius, Y. Alaverdyan, A. Dahlin, F. Hook, D. S. Sutherland, and M. Kall, "Plasmonic sensing characteristics of single nanometric holes," Nano Lett. **5**, 2335–2339 (2005).
3. W. Cai, A. P. Vasudev, and M. L. Brongersma, "Electrically controlled nonlinear generation of light with plasmonics," Science **333**, 1720–1723 (2011).
4. K. Ueno, S. Takabatake, Y. Nishijima, V. Mizeikis, Y. Yokota, and H. Misawa, "Nanogap-assisted surface plasmon nanolithography," J. Phys. Chem. Lett. **1**, 657–662 (2010).
5. K. Ueno, S. Takabatake, K. Onishi, H. Itoh, Y. Nishijima, and H. Misawa, "Homogeneous nano-patterning using plasmon-assisted photolithography," Appl. Phys. Lett. **99**, 011107 (2011).
6. A. V. Zayats, I. I. Smolyaninov, and A. A. Maradudin, "Nano-optics of surface plasmon polaritons," Phys. Rep. **408**, 131–314 (2005).
7. Y. Nishijima, and S. Akiyama, "Unusual optical properties of the Au/Ag alloy at the matching mole fraction," Opt. Mater. Express **2**, 1226–1235 (2012).
8. M. A. Noginov, G. Zhu, A. M. Belgrave, R. Bakker, V. M. Shalaev, E. E. Narimanov, S. Stout, E. Herz, T. Suteewong, and U. Wiesner, "Demonstration of a spaser-based nanolaser," Nature **460**, 1110–1113 (2009).
9. J. Merlein, M. Kahl, A. Zuschlag, A. Sell, A. Halm, J. Boneberg, P. Leiderer, A. Leitenstorfer, and R. Bratschitsch, "Nanomechanical control of an optical antenna," Nat. Photonics **2**, 230–233 (2008).
10. A. Roberts and L. Lin, "Substrate and aspect-ratio effects in resonant nanoaperture arrays," Opt. Mater. Express **1**, 480–488 (2011).

#169179 - $15.00 USD Received 23 May 2012; revised 15 Aug 2012; accepted 4 Sep 2012; published 7 Sep 2012

11. T. J. Davis, M. Hentschel, N. Liu, and H. Giessen, "Analytical model of the three-dimensional plasmonic ruler," ACS Nano **6**, 1291–1298 (2012).
12. Y. Tsuboi, T. Shoji, N. Kitamura, M. Takase, K. Murakoshi, Y. Mizumoto, and H. Ishihara, "Optical trapping of quantum dots based on gap-mode-extinction of localized surface plasmon," Chem. Lett. **1**, 2327–2333 (2010).
13. F. S. Merkt, A. Erbe, and P. Leiderer, "Capped colloids as light-mills in optical traps," New J. Phys. **8**, 216–224 (2006).
14. D. F. P. Pile, T. Ogawa, D. K. Gramotnev, Y. Matsuzaki, K. C. Vernon, K. Yamaguchi, T. Okamoto, M. Haraguchi, and M. Fukui, "Two-dimensionally localized modes of a nanoscale gap plasmon waveguide," Appl. Phys. Lett. **87**, 261114 (2005).
15. M. Osawa, "Dynamic process electrochemical reactions studied by surface-enhanced infrared absorption spectroscopy (SEIRA)," Bull. Chem. Soc. Jpn. **70**, 2861–2880 (1997).
16. N. Ohta, K. Nomura, and I. Yagi, "Electrochemical modification of surface morphology of Au/Ti bilayer films deposited on a Si prism for in situ surface-enhanced infrared absorption (SEIRA) spectroscopy," Langmuir **26**, 18097–18104 (2010).
17. H. Miyatake, E. Hosono, M. Osawa, and T. Okada, "Surface-enhanced infrared absorption spectroscopy using chemically deposited Pd thin film electrodes," Chem. Phys. Lett. **428**, 451–456 (2006).
18. H. Miyatake, S. Ye, and M. Osawa, "Electroless deposition of gold thin films on silicon for surface-enhanced infrared spectroelectrochemistry," Electrochem. Commun. **4**, 973–977 (2002).
19. T. W. Ebbesen, H. J. Lezec, H. F. Ghaemi, T. Thio, and P. A. Wolff, "Extraordinary optical transmission through sub-wavelength hole arrays," Nature **351**, 667–669 (1998).
20. E. Popov, M. Neviere, S. Enoch, and R. Reinisc, "Theory of light transmission through subwavelength periodic hole arrays," Phys. Rev. B **62**, 16100–16108 (2000).
21. H. J. Lezee and T. Thio, "Diffraction evanescent wave model for enhanced and suppressed optical transmission through subwavelength hole arrays," Opt. Express **12**, 3629–3650 (2004).
22. F. J. Garcia-Vidal, L. Martin-Moreno, T. W. Ebbesen, and L. Kuipers, "Light passing through subwavelength apertures," Rev. Mod. Phys. **82**, 729–787 (2010).
23. A. Degiron, H. J. Lezec, N. Yamamoto, and T. W. Ebbesen, "Optical Transmission properties of a single subwavelength aperture in a real metal," Opt. Commun. **239**, 61–66 (2004).
24. H. Rigneault, J. Capoulade, J. Dintinger, J. Wegner, N. Bonod, E. Popov, T. W. Ebbesen, and P. F. Lenne, "Enhancement of single-molecule fluorescence detection in subwavelength apertures," Phys. Rev. Lett. **95**, 117401 (2005).
25. J. Dintinger, S. Klein, and T. W. Ebbesen, "Molecule-surface plasmon interactions in hole allays: enhanced absorption, refractive index changes, and all-optical switching," Adv. Mater. **18**, 1267–1270 (2006).
26. N. Djaker, R. Hostein, E. Devaux, T. W. Ebbesen, H. Rigneault, and J. Wenger, "Surface enhanced Raman scattering on a single nanometric aperture," J. Phys. Chem. C **114**, 16250–16256 (2010).
27. A. Taflove and S. C. Hagness, *Computational Electrodynamics: The Finite-Difference Time-Domain Method*, 3rd ed. (Artech House Publishers, 2005).
28. E. D. Palik, ed., *Handbook of Optical Constants of Solids*, 3rd ed. (Academic Press, 1998).
29. Y. Nishijima, L. Rosa, and S. Juodkazis, "Surface plasmon resonances in periodic and random patterns of gold nano-disks for broadband light harvesting," Opt. Express **20**, 11466–11477 (2012).
30. J. G. Rivas, C. Schotsch, P. H. Bolivar, and H. Kurz, "Enhanced transmission of THz radiation through subwavelength holes," Phys. Rev. B **68**, 201306 (2003).
31. V. Mikhailov, G. A. Wurtz, J. Elliott, P. Bayvel, and A. V. Zayats, "Dispersing light with surface plasmon polaritonic crystals," Phys. Rev. Lett. **99**, 083901 (2007).
32. E. G. Gamaly, "Optical phenomena on the interface between a conventional dielectric and a uniaxial medium with mixed metal-dielectric properties," Phys. Rev. E **51**, 3556–3560 (1995).
33. L. Rosa, K. Sun, V. Mizeikis, S. Bauerdick, L. Peto, and S. Juodkazis, "3D-tailored gold nanoparticles for light field enhancement and harvesting over visible-IR spectral range," J. Chem. Phys. C **115**, 5251–5256 (2011).
34. S. Juodkazis and L. Rosa, "Surface defect mediated electron hopping between nanoparticles separated by a nanogap," Phys. Status Solidi (RRL) **4**, 244–246 (2010).
35. V. Mizeikis, S. Juodkazis, K. Sun, and H. Misawa, "Fabrication of frequency-selective surface structures by femtosecond laser ablation of gold films," J. Laser Micro/Nanoeng. **5**, 115–120 (2010).
36. V. Mizeikis, S. Juodkazis, R. Tarozaitė, J. Juodkazytė, K. Juodkazis, and H. Misawa, "Fabrication and properties of metalo-dielectric photonic crystal structures for infrared spectral region," Opt. Express **15**, 8454–8464 (2007).
37. L. Rosa, K. Sun, and S. Juodkazis, "Sierpinski fractal plasmonic nanoantennas," Phys. Status Solidi (RRL) **5**, 175–177 (2011).

1. Introduction

Surface plasmon resonance on thin metal films has been paid much attention in the fields of chemical sensing [1, 2], optoelectronics [3], and photochemistry [4–6]. Because of a strong lo-

#169179 - $15.00 USD Received 23 May 2012; revised 15 Aug 2012; accepted 4 Sep 2012; published 7 Sep 2012

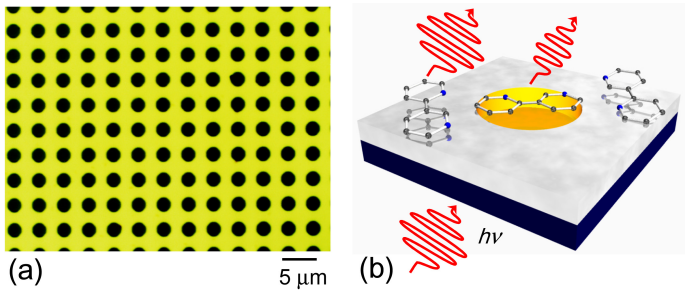

Fig. 1. (a) Optical micro-photograph of the fabricated hole array (MHA) in 100-nm-thick silver where hole diameter $c = 1.65$ μm and period $a \simeq 2c = 3.3$ μm. (b) Schematic illustration of SEIRA caused by localized plasmonic resonance in the micro hole.

calization of electromagnetic field [7], plasmons could lead to non-linear optical phenomena such as two photon absorption, second harmonic generation, surface enhanced Raman scattering (SERS), surface enhanced infrared absorption (SEIRA) and even amplification of emission - the spaser [8]. To achieve a large electromagnetic field enhancement, the size, shape and distance between nano particles has to be controlled with nanometer precision in the nano-gap and bow-tie structures or by using sub-wavelength aperture arrays [9–14]. SERS and SEIRA are promising spectroscopic methods for detection of small amount of molecules and are applicable for DNA, protein and affinity sensors. Within the spectral region of molecular fingerprinting, not only a qualitative analysis, but also the quantitative determination of concentration can be achieved. SERS applications are usually using well-defined gold or silver nanostructures and nanoparticles of well-controlled shape. The chemical and electromagnetic field enhancement effects are both important.

So far, SEIRA measurements were demonstrated only on the rough surface of metal films deposited electrochemically or physically on different substrates [15–18]. The aim of this study is to reveal the relationships between SEIRA and plasmonic resonance effect by using metal hole array (MHA) micro-patterns. MHA, which shows an enhanced transmission at a certain wavelength via coherent scattering of surface plasmon polaritons (SPPs) is one of the well-known plasmonic materials and can be engineered for the enhanced transmission from visible to micro-wave region. The resonance wavelength is mainly defined by periodicity of the holes. The scaling law can be established over different wavelengths similarly to the photonic crystals dispersion. The MHAs are used for applications in optics, terahertz imaging, and biosensing [19–23]. The electromagnetic field enhancement is localized inside of holes, according to the coupling between the incident light and MHA. Using MHA patterns, absorption enhancement of molecules from UV to near-IR wavelength has been reported [24–26]. However, SEIRA functionality at the molecular vibrational region of 200-2000 cm^{-1} (corresponding to 25 meV - 0.25 eV; 50 - 5 μm; 6 - 60 THz) has never been reported. Control and reliable detection of absorption at this IR band is highly required for a low-noise detection of spectra at close to room temperature conditions ($kT \simeq 26$ meV at 20°C), for THz applications, and defect spectroscopy in material science.

Here we show a design of MHAs whose resonance wavelengths can be tuned to the molecular vibrational modes with high selectivity within the 200-2000 cm^{-1} range. The relationship between the absorption enhancement at vibrational modes and resonances of MHA is revealed by experiments and simulations.

#169179 - $15.00 USD Received 23 May 2012; revised 15 Aug 2012; accepted 4 Sep 2012; published 7 Sep 2012

2. Experimental

Designing a MHA structure with resonance wavelength in IR region, fabrication of nano-to-micro-sized holes with specific spatial arrangement has been carried out. MHA structures were fabricated by standard photolithography and lift-off procedure. Silicon substrate (Global top chemical Co. Ltd.) was coated by COAT200 (Tokyo Ohka Kogyo Co. Ltd.) to obtain a hydrophobic surface. Then, a positive type photo-resist (OFPR-500, Tokyo Ohka Kogyo Co. Ltd.) was spin-coated at 3000 rpm for 60 s and pre-baked at 90°C for 90 s. The contact photomask exposure was implemented with UV light using a mask aligner (MA-10, MIKASA Co. Ltd.). After exposure, the samples was developed in 2.38% tetramethyl ammonium hydroxide (NMD-3, Tokyo Ohka Kogyo Co. Ltd.), dried, and coated by 3 nm of Ni adhesion layer followed by 100 nm of Ag using vapor deposition. The following lift-off step in acetone under ultrasonic bath conditions removed resist with excessive metal, then the sample was washed in methanol.

Optical transmission and SEIRA measurements were performed with a Fourier transform IR spectrometer (FTIR-6200 JASCO Co. Ltd.). Azobenzene dye molecules (20 mM in methanol solution) were spin-coated (2000 rpm, 30 s) on the surface of MHA sample. For the reference, a 10-nm-thick Ag film on Si and bare Si substrate were used in IR absorption measurements. The 10 nm Ag film shows strong SEIRA activity [15] and is the limiting thickness for the Ag-film formation. Also, the thin films enhances all the IR absorption bands equally, therefore, we used these films as the reference for the SEIRA on the MHA.

3. Finite difference time domain simulations

The substrate behavior has been simulated by the 3D finite-element time-domain method (3D-FDTD) using the Lumerical software (FDTD Solutions Inc.) The simulation domain is comprised of a Si substrate coated by a 100-nm Ag layer bearing a square lattice of circular holes at constant period; the hole diameter is half the period and the rest of the domain is air. The domain comprises a 11×11 periods portion of the lattice and is enclosed by perfectly-matched layers (PMLs) to avoid edge reflection. The central 5×5 periods are excited by a total-field scattered-field (TFSF) source, assuming that the physical total electric and magnetic fields E_{total} and H_{total} can be decomposed as [27]

$$E_{total} = E_{inc} + E_{scat}; \quad H_{total} = H_{inc} + H_{scat}. \tag{1}$$

E_{inc} and H_{inc} are the known incident fields in an empty simulation domain, while E_{scat} and H_{scat} are the unknown fields scattered by structures in the domain. The FDTD algorithm remains valid for any field due to the linearity of the Maxwell's equations. The domain is thus divided into two distinct regions: inside the TFSF volume the total fields are solved for, while outside the volume the scattered fields are solved for (see Section 4.3 for analysis). The boundaries of the TFSF volume are the nonphysical virtual surfaces connecting the fields in each region, and thereby generating the incident wave. By strictly confining all the structures inside the virtual volume (where the total power can be measured), there is implicitly no incident wave outside that volume itself, and the sole scattering contribution can be measured there. Since the incident power into the source is known, it is possible to establish the power balance and calculate how much power is absorbed by the structures. The outer domain boundary implements a PML to prevent reflection of the scattered field and extend the discretization mesh virtually to infinity. A suitable space is left between the TFSF boundary and the domain boundary to avoid spurious coupling and possible resonances between the discontinuities, albeit small, that these boundaries introduce.

The domain is sampled by a wideband source between 10 and 15 μm wavelength, recording absorption, scattering, and extinction cross-sections, and the E-field intensity enhancement nor-

#169179 - $15.00 USD Received 23 May 2012; revised 15 Aug 2012; accepted 4 Sep 2012; published 7 Sep 2012

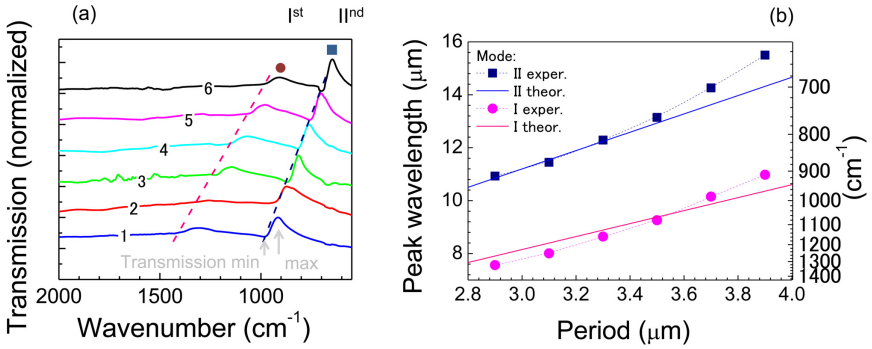

Fig. 2. (a) Experimental transmission spectra of MHA periodic structures with period $a =$ 2.9 to 3.9 μm (2.9 μm (*1*), 3.1 (*2*), 3.3 (*3*), 3.5 (*4*), 3.6 (*5*), 3.9 (*6*) and $c = a/2$ diameter holes; thickness of Ag $d = 100$ nm. Markers show the peak positions of the mode-I (circle) and mode-II (square) transmission maxima; the extinction dip (minima) on the left-side from the peaks is traced by dashed lines. The transmission min-max span is indicated by arrows. Transmission is normalized for better comparison between different samples since the maximum is only 7- 15% transmission in terms of the absolute value. (b) Position of the transmission peak of modes-I,II vs the period c. The linear fit by Eq. (2) is shown by line $\lambda_{max} = 3.466a$ for the major peak $i = 1; j = 0$ and $i = 0; j = 1$ (mode-II) and $\lambda_{max} = 3.466a/\sqrt{2}$ for the minor peak $i = 1; j = 1$ (mode-I).

malized to source intensity. The structure is modeled for periods between 2.9 and 3.9 μm, and the material models are taken from the Lumerical built-in library [28]. The large domain size places computational demands beyond the capabilities of a common desktop machine [29], and simulations are performed using the Green supercomputing Linux cluster at Swinburne University, equipped with 150-plus nodes, each consisting of 8-core processors and 16 GB memory. A typical simulation run takes 6 to 8 hours using 8 nodes and 24 GB memory.

4. Results and discussions

Figure 1 shows an optical micrograph and schematic illustration of SEIRA: a molecular absorption with a MHA sample under halogen lamp illumination; the Ag coated regions appear yellow. Square lattice pattern of holes was used with the lattice period, a, twice large than hole diameter $c = a/2$. When the light was illuminated from the backside of the MHA substrate, a strong enhancement is generated inside the holes and was investigated for SEIRA. An absorption of the azobenzene molecules located in the region of field enhancement is increased (decreasing transmission through the holes) and is experimentally and numerically analyzed below.

4.1. Transmission spectra of multi-hole arrays

The transmission resonance peaks of MHA are dependent on the period and refractive index of surrounding media [25, 30]. We fabricated MHA patterns of different periods from $a = 2.9$ to 3.9 μm on silicon substrate with hole diameters $c = a/2$. Figure 2 shows the transmission spectra of the MHA structures with thickness of silver $d = 100$ nm.

The first and second order resonance peaks are clearly distinguished (Fig. 2(a)). Spectral position of the first order peaks scales linearly with the period and has slope $\gamma \simeq 3.4$, which is related to the refractive index of the silicon substrate (Fig. 2(b)). The peak wavelength is

#169179 - $15.00 USD Received 23 May 2012; revised 15 Aug 2012; accepted 4 Sep 2012; published 7 Sep 2012

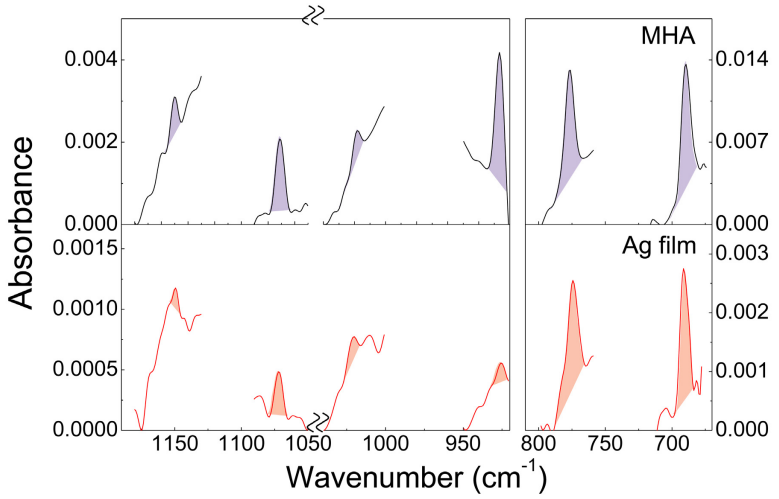

Fig. 3. Surface enhanced infrared absorption (SEIRA) spectra of azobenzene dye on the MHA ($a = 2.9\ \mu$m, $d = 100$ nm, upper row) and on the Ag film (lower row). The baseline of the spectra was strongly modified by the transmission spectra of MHA, hence, only the IR absorption from azobenzene is shown; spectra are collated from measurement over three different spectral windows.

approximately given as [25, 30]:

$$\lambda_{\max} = \frac{a}{\sqrt{i^2 + j^2}} \cdot \sqrt{\frac{\varepsilon_1 \varepsilon_2}{\varepsilon_1 + \varepsilon_2}}, \tag{2}$$

where ε_1 and ε_2 are the dielectric constants of the metal $\varepsilon_1 = -10600 + 2600$i for Ag at 15 μm and the surrounding media $\varepsilon_2 \simeq 12.0$ for Si, respectively, and i and j are diffraction orders in x and y directions of MHA. It is noteworthy, that mode assignment in Fig. 2 is arbitrary and it is not related to the diffraction orders and i, j indices. The positions of the transmission peaks are determined by period and dielectric constant of the substrate. All the MHA transmission peaks are located within the 2000 to 600 cm^{-1} spectral range where vibrational modes of molecules are typically observed in Raman scattering.

The transmission spectra with a 30 and 50 nm thick Ag MHA structures was measured. The position of the transmission peaks was not affected by the silver thickness. This is explained by the following arguments. In the frequency region 18 - 30 THz, the skin depth δ in silver is $\delta = \sqrt{2/\omega\sigma\mu_0}$, where ω is the angular frequency of light, $\mu_0 = 1.256 \times 10^{-6}$ VsA^{-1}m^{-1} is the permeability of free space, and $\sigma = 5.8 \times 10^7$ S/m is the electric conductivity of silver, respectively. One would find that $\delta \simeq 12 - 15$ nm; hence, the thickness of Ag-film is larger than the skin depth. Surface plasmon polaritons (SPPs) can only propagate on the surface within the skin depth, with exponentially decreasing intensity towards the interior. So, there is no interaction between SPPs on the front and back sides of the Ag surface.

4.2. SEIRA spectra of azobenzene dye molecules on multi-hole arrays

Most of all SEIRA spectroscopic studies have been carried out on the rough surfaces of thin metallic films or nano-island structures which are deposited as few-nm-thick metal films by thermal evaporation, sputtering, or electrochemically etching the surface of metal [6, 21]. In

#169179 - $15.00 USD Received 23 May 2012; revised 15 Aug 2012; accepted 4 Sep 2012; published 7 Sep 2012

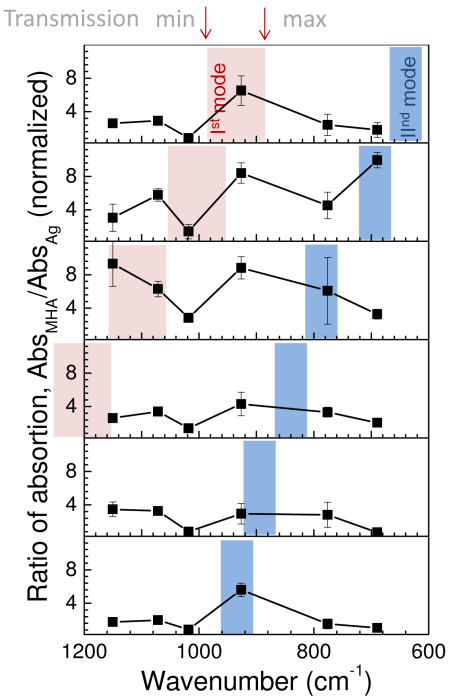

Fig. 4. Experiment: SEIRA enhancement spectrum on a MHA substrate with period from $a = 2.9$ to 3.9 μm and hole diameter $c \equiv a/2 = 1.45$ to 1.95 μm (from bottom upwards, same periods as in Fig. 2), Ag thickness $d = 100$ nm) normalized to the absorption on an unstructured Ag film. The shaded regions show the width of the transmission minimum and the maximum span according to Fig. 2(a); marked by arrows on the top.

these studies, not only specific vibrational modes but rather all vibrational absorption peaks are enhanced by the rough surface. The MHA structures, however, have electromagnetic field enhancement at specific frequencies, and this can be used to enhance specific absorption peaks of vibration modes of molecules at infrared wavelengths.

Figure 3 shows SEIRA spectra of azobenzene molecules on the MHA and on the silver metal film of 10 nm thickness. From 1200 to 600 cm^{-1}, we can find six vibrational modes of azobenzene. As a reference for the MHA structure, infrared absorption on Ag film is also shown (lower row in Fig. 3). Clearly, the absorbance on the MHA is increased as compared with that on an even Ag film. The enhancement factor appears different for the individual peaks as would be expected due to the difference in selection rules of the vibrations. The absorption of the dye on a bare silicon substrate was measured, however, there where no absorption peaks detectable. Although we have not characterized the roughness of our Ag thin film, from this result we can conclude that the MHA could be useful and is more sensitive for detection of small amount of molecules as compared to the Ag thin film used in typical SEIRA studies.

Figure 4 shows the absorption enhancement of dye on the MHA sample as compared to that on Ag film vs the absorption wavenumber; the spectral positions of transmission peaks of MHA are marked. In the most cases, When the 1st peak of MHA transmission was overlapped with the azobenzene absorption peaks, the absorbance increased because of electromagnetic field enhancement in the MHA. However, there were exceptions, e.g., second row in Fig. 4; this is attributable to the symmetry of the vibration which determines coupling with light field (discussed in the next paragraph). Even at the position of the 2nd transmission peak of MHA,

#169179 - $15.00 USD Received 23 May 2012; revised 15 Aug 2012; accepted 4 Sep 2012; published 7 Sep 2012

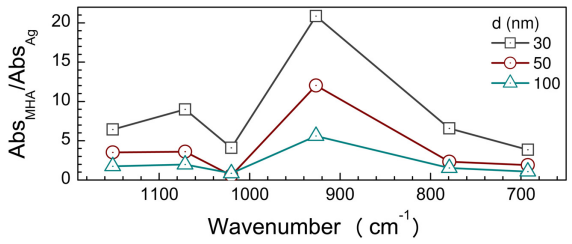

Fig. 5. SEIRA enhancement on MHA with $a = 2.9$ μm period and different thickness of Ag film $d = 30, 50$ and 100 nm.

a weak enhancement of the dye absorption occurred. The difference of electromagnetic field enhancement between the first and second peaks is discussed next.

In the window between 950 and 1150 cm^{-1}, the absorption peaks always seem to be enhanced in all of the MHA structures (Fig. 4). From calculations using a molecular orbital method (by software MOPAC), the 950 and 1150 cm^{-1} absorption peaks were i defined as angular oscillations of outer plane of π-conjugation of benzene and azo-group. The other four peaks (Fig. 3) are due to oscillations of inner plane in π-conjugation. This calculation result indicates that the orientation of molecules matters and for some particular vibration modes coupling between light and vibrations is weak. This is a reflection of a well known feature determined by selection rules of absorption and scattering.

For comparison, SEIRA was measured using attenuated-total-reflection (ATR) geometry, however, no enhancement was observed. This is caused by phase matching of plasmons in MHA structures and the incident light. Previous plasmonic crystal studies [31] indicated that there is a particular angular dependence of plasmonic resonance in MHA samples. The normal incidence used in this study is favorable for the maximum enhancement for the throughout-holes extraordinary transmission [19].

Though the skin depth on Ag is only ~ 15 nm, and coupling between SPPs on two sides of uniform Ag film is not taking place, it becomes different for the perforated film - the MHA samples. Thickness dependence of enhancement in MHA structures was investigated and is summarized in Fig. 5. MHA transmission resonance strongly depends on the periodicity of the holes, and the dielectric constant of metal, substrate and surrounding environment. It is less sensitive to the thickness of metal film due to skin depth, as discussed earlier. By decreasing the thickness of the MHA film, the absorption enhancement become larger (Fig. 5). Experimentally, fabricating Ag films less than 20 nm thick with smooth surface becomes challenging due to granular pattern and dewetting at larger surface temperatures. Hence, we show results in Fig. 5 for Ag films with the same surface roughness.

4.3. Numerical simulations of transmission of multi-hole arrays

To clarify the electromagnetic field enhancement of MHA samples, we have performed FDTD calculations on the geometrical parameters of the actual structures.

Figure 6 depicts the FDTD calculation results for the case where the period is 3.7 μm (hole diameter = 1.85 μm), in which the extinction of mode II is maximum according to Fig. 4. The cross-section plots in Fig. 6(a) correlate well with the experimental results in Fig. 2(a): where in the experiment the transmission shows a minimum followed by a maximum, and a weak mode I followed by a stronger mode II, in the cross-section plot we see extinction maxima (transmission is reduced) followed by surface E-field enhancement maxima (transmission is enhanced) indicated by the colored markers, giving rise to bands similar to Fig. 4. The simulation predicts the existence of a lower-energy mode III which shows more prominently at large period values,

#169179 - $15.00 USD Received 23 May 2012; revised 15 Aug 2012; accepted 4 Sep 2012; published 7 Sep 2012

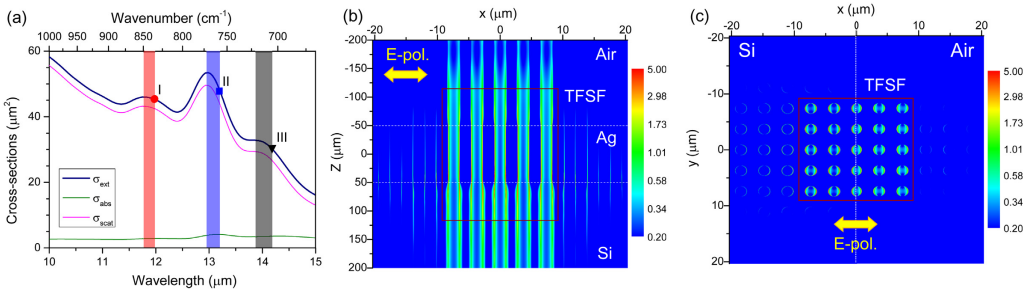

Fig. 6. Numerical simulations. (a) Cross-sections for period = 3.7 μm (hole diameter = 1.85 μm). The TFSF source encompasses 25 holes (5×5 lattice periods) and its total-field region indicated by the pink square in (b,c). The geometrical cross-section of one hole is 2.688 μm^2, for 25 holes it is 67.2 μm^2. The geometrical cross-section of the metal surface minus the holes is 275.05 μm^2. The markers indicate the maximum field enhancement wavelengths for the three resonant modes, and the colored bars show the bandwidth extension between the min transmission (max extinction) and max transmission (max field enhancement) wavelengths. Mode-II: (b) *xz*-plane $|E|^2$ enhancement log-plot, revealing the thin enhancement layers in the total-field region and the *x*-directed long-range plasmon coupling in the scattered-field region; (c) *xy*-plane $|E|^2$ enhancement log-plot showing metal interface distributions on Si-side (left half of the panel, max enhancement = 32) and Air-side (right half of the panel, max enhancement = 11). The scale has been restricted in the log-plots to mitigate color blooming.

presumably too weak to show in the experiment. Scattering is higher in the neighborhood of the extinction maxima as absorption is fairly constant in the band. The normalized $|E|^2$ field intensity distribution at the 13.2 μm peak enhancement wavelength is shown in Figs. 6(b) and 6(c); the stronger enhancement at the Ag-Si interface with respect to the Air-Ag interface (32 vs. 11 normalized) is seen in the central region of the log-scale plot in Fig. 6(b), where the total field is solved for in the TFSF formulation as described in Section 3, while in the outer region the solution for the scattered field is shown, emphasizing the long-range plasmonic coupling between the holes, where energy flows according to the incident wave polarization. The *xz*-plane $|E|^2$ section in Fig. 6(c) shows how the field is strictly confined along the hole walls but extends significantly into the air and substrate. The scattered waves travel mainly along the metal-substrate interface. It has been predicted, that at certain periodicity of 2D pattern on a metal film, a long range propagating SPPs can be launched [32]. This can be used to enhance sensitivity of the MHA structures in real applications.

Figure 7 shows results of FDTD calculations for the MHA extinction peak wavelength and electromagnetic field enhancements at two different locations: the top surface and at the interface between Si substrate and Ag film with holes. The extinction peaks are named according to the transmission modes (see, Fig. 2(a)). The peak wavenumbers of the three modes decrease with period (Fig. 7(a)) with a trend similar to the experiment (Fig. 2(a)). Usually, the extinction peak corresponds to the spectral position where the field enhancement is maximum in the case of plasmonic nanoparticles [33, 34]. However, it was found that in the case of hole arrays, the transmission maximum wavelength defines the maximum field enhancement and, consequently, the SEIRA enhancement rather than the extinction peak (even the transmission and extinction peaks are close to each other as shown in Fig. 6). The surface enhancement evolution for mode II in Fig. 7(b) is well-correlated with the results in Fig. 4, showing a sharp maximum for a period of 3.7 μm. This is an indication that the azobenzene spin-coated on the hole array is, most probably, not penetrating into the holes, where the highest enhancement of 43 is reached

#169179 - $15.00 USD Received 23 May 2012; revised 15 Aug 2012; accepted 4 Sep 2012; published 7 Sep 2012

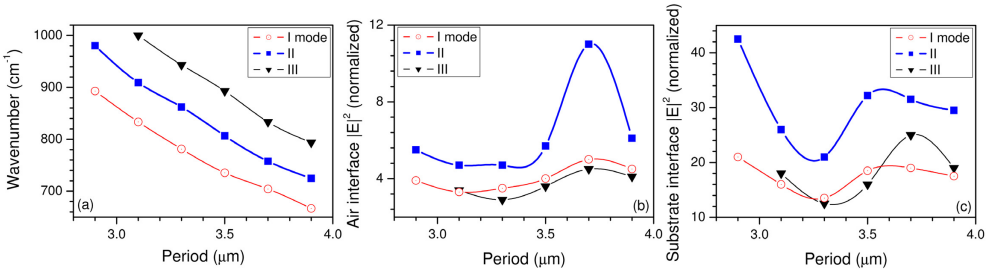

Fig. 7. Summary of the 3D-FDTD calculations for the extinction maximum peak wavelength in wavenumbers cm^{-1} (a) and $|E|^2$ enhancement factors at the top air-Ag (b) and interface Si-Ag (c) planes. These extinction peaks are related to the transmission modes I, II, and III in correspondence with Figs. 2 and 4.

at a period of 2.9 μm on the Si-Ag interface according to Fig. 7(c). Indeed, spin coated films tend not to enter holes filled with air. Since we did not used desiccators nor low pressure during film deposition, the azo-dye molecules are preferentially on the top of the surface with a small fraction present near the hole rims where light fields are enhanced.

The hole array sensors are promising for gas sensing applications when analyte molecules naturally enter the hot spots at substrate-Ag interface inside holes. It is also noteworthy, that some of the IR absorption bands can be inactivated on the flat surfaces and the experimental spectra (Fig. 4) are not exactly following the field enhancement predictions (Fig. 6). The holes larger than 1 μm in diameter can be made using simpler mask projection lithography, laser ablation, and ion beam lithography [33,35]. Also, the IR edge filters can be made using metallic coating on polymerized photonic crystals [36]. This opens a possibility to selectively excite particular IR modes of molecular absorption.

5. Conclusion

In this study, we have successfully fabricated MHA micro-structures for IR molecular vibration region with large area by lithography and lift off. The enhancement of the vibrational absorption modes of molecules at IR (sub-THz 10 - 20 THz) wavelengths. The MHA structure shows strong electromagnetic field enhancement up to $\sim$ 20-times at a narrow specific frequency. In that frequency range the enhancement of 10 times as high as on a 10-nm-thick silver film surface was observed. For the analyte molecules entering the holes the enhancement factor is expected to be even larger by 2-3 times, as the modelled MHA structure is predicted to have maximum surface intensity enhancement of 11, and 32 at the Au-Si interface, going as high as 43.

Specific absorption peaks of molecular vibration are enhanced selectively (up to an order of magnitude) when the absorption coincides with the transmission peak of the MHA pattern. The electromagnetic field enhancement generated in MHA is selectively enhancing the vibrational modes. Enhancement factor of MHA structures is expected to be enlarged in the nano/micro composite structures such as fractals [37]. These micrometer-sized MHA devices, which are amenable with inexpensive and already well-established techniques, can be applied to the chemical reactions with selective group excitation for controlling side-reaction products, controlling of partial unfolding of biomaterials like proteins and DNA.

#169179 - $15.00 USD Received 23 May 2012; revised 15 Aug 2012; accepted 4 Sep 2012; published 7 Sep 2012

Acknowledgments

The authors are grateful to Prof. T. Baba from Yokohama Nat. Univ. for fruitful discussions and for granting access to fabrication facilities. We thank Tokyo Ohka Kogyo Co. Ltd. for providing photoresist and surfactant used for fabrication, and Instrumental Analysis Center (Yokohama Nat. Univ.) for FTIR measurements. This work was financially supported by the Ministry of Education, Culture, Sports, Science, and Technology: KAKENHI Grant-in-Aid for scientific research, the Yokohama Academic Foundation, and the Research Foundation for Optical Science and Technology, Hamamatsu, Japan. SJ is grateful for support via DP120102980 grant from the Australian Research Council.

#169179 - $15.00 USD Received 23 May 2012; revised 15 Aug 2012; accepted 4 Sep 2012; published 7 Sep 2012